ISSN 1995-4239, Numerical Analysis and Applications, 2020, Vol. 13, No. 2, pp. 136–151. © Pleiades Publishing, Ltd., 2020.
Russian Text © The Author(s), 2020, published in Sibirskii Zhurnal Vychislitel'noi Matematiki, 2020, Vol. 23, No. 2, pp. 165–181.

Finite Element Method for the Stokes–Darcy Problem with a New Boundary Condition

O. El Moutea[1*], H. El Amri[1], and A. El Akkad[2]**

[1] *Ecole Normale Supérieure Casablanca, Faculté des Sciences Aïn Chock Université Hassan II, Route d'El Jadida, km. 9, Ghandi-Casablanca, 50069, Morocco*

[2] *Centre Régional des Métiers d'Education et de Formation de Fès Meknès, Rue de Koweit 49, Fés, 30050, Morocco*

Received February 5, 2019; in final form, April 10, 2019; accepted December 19, 2019

Abstract—This paper considers numerical methods for approximating and simulating the Stokes–Darcy problem, with a new boundary condition. We study a robust stabilized fully mixed discretization technique. This method ensures stability of the finite element scheme and does not use any Lagrange multipliers to introduce a stabilization term in the temporal Stokes–Darcy problem discretization. A correct finite element scheme is obtained and its convergence analysis is done. Finally, the efficiency and accuracy of these numerical methods are illustrated by different numerical tests.

DOI: 10.1134/S1995423920020056

Keywords: *Stokes–Darcy problem, mixed finite element method, free flow, porous media flow, stabilized scheme.*

1. INTRODUCTION

In this article, we focus on the study of fluid flow in different domains and different physical situations, for example, coupling of groundwater and surface flows, which is coupling of both surface and subsurface flows. This model is described with the Stokes–Darcy equation. This relationship is provided by the Stokes–Darcy linear equations with a contact interface. The Beavers and Joseph interface conditions in the Stokes–Darcy model, which have become a most important topic in research, can be found in [9–11]. Saffman modified this interface condition in [7, 40]. This model arises in the hydrology, particularly, in groundwater flows, and in modeling of reservoirs in petroleum engineering. It is also used for describing many natural and industrial phenomena in biomedicine and industrial processes [1, 7].

In different approximations, the Stokes–Darcy equations differ. A lot of effort and many techniques have been applied in this connection to conduct numerical simulations (see [2, 3, 7, 33, 35, 44, 45]). During the last decades, study of this problem has received a lot of attention, in particular related to a flow in porous media In this case, there are several ways to define error estimators for these Stokes equations by using the residual equation (see [2, 24]). Solving the Stokes equations and Navier–Stokes equations governing a steady flow of viscous incompressible fluid can be found in [7, 28, 29]. These works laid the basic foundation for approximation of coupled Navier–Stokes equations. In [17], Cao, Gunzburger, He, and Wang investigated decomposition methods for a steady-state Stokes–Darcy system. A locally conservative numerical method was applied to investigate coupled free and porous flow media in [23], where the discontinuous Galerkin finite element method was applied to the Stokes region and the mixed finite element method was used for the Darcy domain. A study with different cavities on the microscopic scale using the Stokes model equations and the finite element method was performed by Arbogast et al. in [4]. In [35], decoupled schemes for a non-stationary model were investigated. The unified stabilized method was studied by Burman et al. [14]. Pearson, Pestana, and Silvester applied the refined saddle-point preconditioning technique in [37] . Camaño, Gatica, Oyarzúa, Ruiz-Baier, and Venegas [16] used

[*] E-mail: mouteaomar@gmail.com
[**] E-mail: elakkadabdeslam@yahoo.fr

new fully-mixed finite element methods for the coupled Stokes–Darcy equations. The reader can find more works on the mixed formulation in [12, 16].

The rest of this paper is organized as follows. In Section 2, we give a short description of the Stokes–Darcy fluid flow model with the Beavers–Joseph interface conditions. In Section 3, we give some notations and the variational formulation for our problem. The numerical scheme for the model is presented in Section 4. The stabilized finite element method and its stability will be discussed in Section 5. The proof of our main result, i.e., error estimation for the coupled schemes, and analysis of the finite element scheme are given in Section 6. Finally, in Section 7, we present $2D$ numerical tests to show the accuracy of the numerical methods.

2. THE MODEL PROBLEM

It is of interest for us to consider a model that couples subsurface water and surface flows via the Stokes–Darcy equations. Using these equations, we can model different domains and physical situations to simulate realistic problems. These problems are presented by partial differential equations, coupled in the interface.

Let Ω_f and Ω_p be two bounded domains of $\mathbb{R}^d$ $(d = 2, 3)$, lying on both sides of an interface Γ, where $\Omega_f \cap \Omega_p = \emptyset$, $\bar{\Omega}_f \cap \bar{\Omega}_p = \Gamma$, and $\bar{\Omega}_f \cup \bar{\Omega}_p = \Omega$. Note that n_f and n_p are the unit outward normal vectors on $\partial\Omega_f$ and $\partial\Omega_P$,respectively; $(\tau_i)_{i=1,\cdots,d-1}$ are the unit tangent vectors to Γ, $\Gamma_f = \partial\Omega_f \backslash \Gamma$ and $\Gamma_p = \partial\Omega_p \backslash \Gamma$ (see Fig. 1). To address the problem mentioned above, let $n_p = -n_f$. Let us make clear some notations that are introduced in this section and will be used in the remaining of this paper. Recall that ∇ and $\nabla\cdot$ are the gradient and divergence operators, respectively.

2.1. The Stokes Equation

Let $u_f(x)$ be the fluid velocity, $p(x)$ the pressure, and μ a positive constant of viscosity. Consider the following Stokes model:

$$\begin{cases} -\nabla^2 \mu\, u_f + \nabla p = f & \text{in } \Omega_f, \\ \nabla \cdot u_f = 0 & \text{in } \Omega_f, \end{cases} \tag{1}$$

with a new boundary condition

$$C_{\mu,\beta} : \beta u_f + (\nabla \mu u_f - pI)\, n_f = g_f. \tag{2}$$

Here $f(x) \in (L^2(\Omega))^2$, $g_f(x) \in (L^2(\Omega))^2$, $p\,(x) \in L^2(\Omega)$, and β is a non-zero bounded continuous function defined on Γ_f. $C_{\mu,\beta}$ will be called the *Dirichlet condition* if $\beta \gg 1$ and the *Neumann condition* if $\beta \ll 1$.

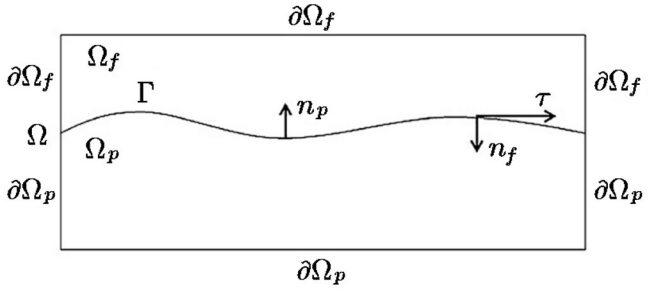

Fig. 1. Problem domain Ω, consisting of fluid region Ω_f and porous medium region Ω_p, separated by interface Γ.

2.2. The Darcy Equations

A porous media flow is governed by the following Darcy equation on Ω_p at the fluid velocity $u_p(x)$ and the piezometric head $h(x)$:

$$\begin{cases} u_p = -K\nabla h & \text{in } \Omega_p, \\ \nabla \cdot u_p = f_p & \text{in } \Omega_p, \end{cases} \tag{3}$$

with the boundary condition

$$u_p \cdot n_p = g_p \text{ on } \Gamma_p. \tag{4}$$

In this case, $f_p(x), g_p(x) \in L^2(\Omega)$, and the piezometric head $h(x)$ is an element of $L^2(\Omega)$.

We introduce the following notation: f denotes the body forces in the fluid region, f_p is the source region in the porous media, K is the hydraulic conductivity tensor, μ is the viscosity of the fluid, and α is a constant parameter. Assume that all material and fluid parameters are uniformly positive and bounded and K is a symmetric positive matrix. Then

$$0 \le k_{\min}|\zeta|^2 \le K\,\zeta \cdot \zeta \le k_{\max}|\zeta|^2 < \infty \text{ for all } \zeta \in (\mathbb{R})^d.$$

2.3. Interface Coupling

In this part, we consider the well-known Beavers–Joseph interface condition on the interface Γ (see [8, 13] for more details):

$$\begin{cases} u_p \cdot n_p + u_f \cdot n_f = 0 & \text{on } \Gamma, \\ p - \mu n_f\, \nabla u_f \cdot n_f = \rho g h & \text{on } \Gamma, \\ -n_f \cdot \nabla u_f \cdot \tau_i = \frac{\alpha}{\sqrt{\tau_i \cdot K \tau_i}} u_f \cdot \tau_i & \text{on } \Gamma, \end{cases} \tag{5}$$

with $1 \le i \le d-1$. Equations (5) is a simplification of the more unconventional and realistic Beavers–Joseph conditions, where $u_f \cdot \tau_i$ is replaced by $((u_f - u_p) \cdot \tau_i)$ (see also [6]).

3. NOTATIONS AND THE VARIATIONAL FORMULATION

In this section, we first introduce some results about Sobolev spaces (see [1, 43]). Assume $\|\cdot\|$ is the usual L^2-norm for functions defined on Ω_f or Ω_p, which is set as follows:

$$\begin{aligned} \|p\| &= \left(\int_{\Omega_f} |p|^2 \right)^{\frac{1}{2}} \text{ for all } p \in L^2(\Omega_f), \\ \|v_f\| &= \left(\sum_{i=1}^{d} \int_{\Omega_f} |v_f^i|^2 \right)^{\frac{1}{2}} \text{ for all } v_f \in \left(L^2(\Omega_f)\right)^d, \\ \|\nabla v_f\| &= \left(\sum_{i=1}^{d} \int_{\Omega_f} |\nabla v_f^i|^2 \right)^{\frac{1}{2}} \text{ for all } v_f \in \left(L^2(\Omega_f)\right)^d, \end{aligned} \tag{6}$$

and $(\cdot,\cdot)$ is the corresponding inner product over the interface Γ, as follows:

$$(p,q)=\int_{\Gamma} p\cdot q\,d\Gamma. \tag{7}$$

Let H_{div} be the space of vector fields $H(\Omega_p)$ with components in $(L^2(\Omega_p))^d$:

$$H_{\text{div}}=H(\text{div},\Omega_p)=\left\{v_p\in(L^2(\Omega_p))^d:\nabla\cdot v_p\in(L^2(\Omega_p))^d\right\}. \tag{8}$$

We are in position to introduce (following [4, 13]) the spaces

$$\begin{aligned}
&X_f=\left(H_0^1(\Omega_f)\right)^2,\\
&Q_f=\left\{q\in L^2(\Omega_f),\int_{\Omega_f}q(x)\,dx=0\right\},\\
&Q_p=L^2(\Omega_p),\\
&X_p=\{v_p\in H_{\text{div}},\ \nabla v_p\cdot n_p=g\}.
\end{aligned} \tag{9}$$

The spaces X_f and X_p are equipped with the following norms:

$$\begin{aligned}
\|v_f\|_1&=(\|v_f\|+\|\nabla v_f\|)^{\frac{1}{2}}\ \text{ for all }\ v_f\in X_f,\\
\|v_p\|_{\text{div}}&=(\|v_p\|+\|\nabla v_p\|)^{\frac{1}{2}}\ \text{ for all }\ v_p\in X_p.
\end{aligned} \tag{10}$$

The variational formulation of steady-state Stokes–Darcy problems (1)–(3) with new boundary conditions (2) and (4) can be written as follows: Find $(u_f,p;u_p,h)\in(X_f,Q_f;X_p,Q_p)$ that satisfy the following conditions:

$$\begin{cases}
a_f(u_f,v_f)-b_f(v_f,p)+c_\Gamma(v_f,h)=L_f(v_f),\\
b_f(u_f,q)=0
\end{cases} \tag{11}$$

for all $(v_f,q)\in X_f\times Q_f$ and

$$\begin{cases}
a_p(u_p,v_p)-b_p(v_p,h)-c_\Gamma(v_p,h)=0,\\
b_p(u_p,\psi)=\rho g(f_p,\psi)
\end{cases} \tag{12}$$

for all $(v_p,\psi)\in X_p\times Q_p$, where

$$\begin{aligned}
&a_f(u_f,v_f)=a_1(u_f,v_f)+a_\Gamma(u_f,v_f),\\
&a_1(u_f,v_f)=\mu\int_{\Omega_f}\nabla u_f\cdot\nabla v_f+\sum_{i=1}^{d-1}\frac{\alpha}{\sqrt{\tau_i\cdot K\tau_i}}(u_f\cdot\tau_i,v_f\cdot\tau_i),\\
&a_\Gamma(u_f,v_f)=\int_{\Gamma}\beta u_f\cdot v_f,\\
&b_f(v_f,p)=(p,\nabla\cdot v_f),\\
&c_\Gamma(v_f,h)=\rho g(h,v_f\cdot n_f)_\Gamma,\\
&a_p(u_p,v_p)=\rho g\left(K^{-1}u_p,v_p\right),\\
&b_p(v_p,h)=\rho g(h,\nabla\cdot v_p),\\
&L_f(v_f)=(f_f,v_f)+\int_{\Gamma}g_f\cdot v_f,
\end{aligned}$$

in the sense that

$$\begin{aligned} L\left(u_f, p, u_p, h; v_f, q, v_p, \psi\right) = {} & a_f\left(u_f, v_f\right) - b_f\left(v_f, p\right) + b_f\left(u_f, q\right) \\ & + a_p\left(u_p, v_p\right) - b_p\left(v_p, h\right) + b_p\left(u_p, \psi\right) + c_\Gamma\left(v_f - v_p, h\right). \end{aligned} \tag{13}$$

Equations (11) and (12) are equivalent to the following:

$$\begin{cases} \text{Find} \quad \left(u_f, p; u_p, h\right) \in \left(X_f, Q_f; X_p, Q_p\right) \quad \text{that satisfy} \\ L\left(u_f, p, u_p, h; v_f, q, v_p, \psi\right) = \rho g\left(f_p, \psi\right) + L_f\left(v_f\right) \\ \text{for all} \quad \left(v_f, q; v_p, \psi\right) \in \left(X_f, Q_f; X_p, Q_p\right). \end{cases} \tag{14}$$

It is easy to check that (14) is uniquely-defined (see [21, 45]).

Recall also the Poincaré, Korn, and trace inequalities, which will be used in the next section: there exist constants C_P, C_K, and C_v that depend only on the spaces and are such that for all $v_f \in X_f$

$$\left\|v_f\right\| \leq C_P \left|v_f\right|_1, \tag{15}$$

$$\left|v_f\right|_1 \leq C_K \left\|\nabla v_f\right\|, \tag{16}$$

and for all $v_f \in L^2\left(\Gamma\right)$,

$$\left\|v_f\right\|_{L^2(\Gamma)} \leq C_v \left|v_f\right|_1^{\frac{1}{2}} \left\|v_f\right\|^{\frac{1}{2}}. \tag{17}$$

Similarly, there exist constants $\tilde{C}_v$ that depend only on Ω_p and are such that for all $\psi \in Q_p$

$$\left\|\psi\right\|_{L^2(\Gamma)} \leq \tilde{C}_v \left|\psi\right|_1^{\frac{1}{2}} \left\|\psi\right\|^{\frac{1}{2}}. \tag{18}$$

Hereafter, all the constants are positive unless otherwise specified.

4. NUMERICAL SCHEME

Consider a family of triangulations $T_h = T_h^f \cup T_h^p$ for $\Omega = \Omega_f \cup \Omega_p$, separated by the interface Γ, where T_h^f and T_h^p are regular triangulations of Ω_f and Ω_p,respectively. For uniformly regular triangulation, $\overline{\Omega} = \bigcup_{K \in T_h} K$ and there exist positive constants c_1 and c_2 such that

$$c_1 h \leq h_K \leq c_2 \rho_K$$

for approximation of the diameter h_K of the triangle (tetrahedral) K and the diameter ρ_K of the ball included in K, where h is a positive parameter defined as $h = \max_{K \in T_h} h_K$.

From the parts T_h^f and T_h^p, for T_h we define finite element spaces $X_{fh} \subset X_f$, $Q_{fh}^h \subset Q_f$, $X_{ph} \subset X_p$, and $Q_{ph} \subset Q_p$. We also consider the well-known MINI elements (P1b–P1) to approximate the velocity and pressure in the Stokes equation (see [44]). The fully mixed technique uses Lagrangian elements P1 for the hydraulic (piezometric) head and Brezzi–Douglas–Marini piecewise constant finite elements BDM1 for the Darcy velocity (see [45]). For the Stokes problem in the fluid flow region, we select finite element spaces $\left(X_{fh}, Q_{fh}\right)$ that satisfy the inf–sup condition: there exists a constant $\beta_f > 0$ (independent of h) such that

$$\inf_{q^h \in Q_{fh},\, q^h \neq 0} \sup_{v_f^h \in X_{fh},\, v_f^h \neq 0} \frac{b_f\left(v_f^h, q^h\right)}{\left|v_f^h\right|_1 \left\|q^h\right\|} \geq \beta_f \tag{19}$$

for all $v_f^h \in X_{fh}$ and $q^h \in Q_{fh}$.

In the porous region, we use finite element spaces (X_{ph}, Q_{ph}) that satisfy the standard inf–sup condition: there exists a constant $\beta_p > 0$ such that for all $q^h \in Q_{ph}$

$$\beta_p \|q^h\| \leq \sup_{v_p^h \in X_{ph}, v_p^h \neq 0} \frac{b_p(v_p^h, q^h)}{\|v_p^h\|_{\text{div}}}. \tag{20}$$

From assumption (19) and for an arbitrary (but fixed) pressure p^h in Q_{fh}, we get a function w_f^h in X_{fh} such that

$$b_f\left(w_f^h, p^h\right) \geq \tilde{C}_1 \|w_f^h\|_1 \|p^h\|, \tag{21}$$

where w_f^h is normalized as $\|w_f^h\|_1 = \lambda_1 \|p^h\|$. We have

$$b_f\left(w_f^h, p^h\right) \geq C_1 \|p^h\|^2. \tag{22}$$

Similarly, from assumption (20) and for $h^h \in Q_{ph}$, we get that there exists $w_p^h \in X_{ph}$ such that

$$b_p\left(w_p^h, h^h\right) \geq \tilde{C}_2 \|w_P^h\|_{\text{div}} \|h^h\|. \tag{23}$$

By normalizing it so that $\|w_p^h\|_{\text{div}} = \lambda_2 \|h^h\|$, we have

$$b_p\left(w_p^h, h^h\right) \geq C_2 \|h^h\|^2. \tag{24}$$

Finally, there exist two constants C_{inv} and $\tilde{C}_{\text{inv}}$ depending on the minimum angles of the mesh in Ω_f and Ω_p such that

$$|v_f^h|_1 \leq C_{\text{inv}} h^{-1} \|v_f^h\| \text{ for all } v_f^h \in X_{fh}, \tag{25}$$

$$|\psi^h|_1 \leq \tilde{C}_{\text{inv}} h^{-1} \|\psi^h\| \text{ for all } \psi^h \in Q_{ph}. \tag{26}$$

These inequalities in X_{fh} and Q_{ph} will be useful in the sections below.

5. STABILITY OF THE METHOD

In this section, we will mostly work with the stabilized finite element scheme for our problem, in the sense that

$$\begin{cases} \text{Find } \left(u_f^h, p^h; u_p^h, h^h\right) \in (X_{fh}, Q_{fh}; X_{ph}, Q_{ph}) \text{ satisfying} \\ \tilde{L}\left(u_f^h, p^h, u_p^h, h^h; v_f^h, q^h, v_p^h, \psi^h\right) = \rho g\left(f_p, \psi^h\right) + L_f\left(v_f^h\right) \\ \text{for any } \left(v_f^h, q^h, v_p^h, \psi^h\right) \in (X_{fh}, Q_{fh}; X_{ph}, Q_{ph}), \end{cases} \tag{27}$$

where

$$\begin{aligned} \tilde{L}\left(u_f^h, p^h, u_p^h, h^h; v_f^h, q^h, v_p^h, \psi^h\right) = L\left(u_f^h, p^h, u_p^h, h^h; v_f^h, q^h, v_p^h, \psi^h\right) \\ + \frac{\delta}{h}\left(\left(u_f^h - u_p^h\right) \cdot n_f, \left(v_f^h - v_p^h\right) \cdot n_f\right)_\Gamma \end{aligned} \tag{28}$$

The stabilization term for the Stokes–Darcy problem is

$$\frac{\delta}{h}\left(\left(u_f^h-u_p^h\right)\cdot n_f,\left(v_f^h-v_p^h\right)\cdot n_f\right)_\Gamma=\frac{\delta}{h}\int_\Gamma\left(\left(u_f^h-u_p^h\right)\cdot n_f\right)\left(\left(v_f^h-v_p^h\right)\cdot n_f\right)d\Gamma.$$

In order to prove the stability of finite element scheme (27), let us define the norm

$$\left|\left\|u_f^h,p^h,u_p^h,h^h\right\|\right|=\left\|u_f^h\right\|_1+\left\|p^h\right\|+\left\|u_p^h\right\|_{\mathrm{div}}+\left\|h^h\right\|+h^{-\frac{1}{2}}\left\|u_f^h-u_p^h\right\|_\Gamma, \tag{29}$$

and prove the continuity and coercivity of problem (28).

(i) Continuity of the stabilized finite element scheme.

Theorem 1. *There exists a constant C such that*

$$\tilde{L}\left(u_f^h,p^h,u_p^h,h^h;v_f^h,q^h,v_p^h,\psi^h\right)\le C\left(\left|\left\|u_f^h,p^h,u_p^h,h^h\right\|\right|\right)\left(\left|\left\|v_f^h,q^h,v_p^h,\psi^h\right\|\right|\right) \tag{30}$$

holds for all $\left(v_f^h,q^h,v_p^h,\psi^h\right)\in(X_{fh},Q_{fh},X_{ph},Q_{ph})$.

Proof. By using Schwartz inequality (18) and inverse inequality (25) for $a_\Gamma\left(u_f^h,v_f^h\right)$, we have

$$a_\Gamma\left(u_f^h,v_f^h\right)\le C_1\left\|u_f^h\right\|\left\|v_f^h\right\|, \tag{31}$$

where $C_1=h^{-\frac{1}{2}}C_{\mathrm{inv}}^{\frac{1}{2}}C_v$. This ensures that

$$a_f\left(u_f^h,v_f^h\right)\le(1+C_1)\left\|u_f^h\right\|\left\|v_f^h\right\|.$$

Similarly, for $c_\Gamma\left(u_f^h-u_p^h,h^h\right)$ and $\frac{\delta}{h}\left(\left(u_f^h-u_p^h\right)\cdot n_f,\left(v_f^h-v_p^h\right)\cdot n_f\right)_\Gamma$, we obtain

$$c_\Gamma\left(u_f^h-u_p^h,h^h\right)\le C_2h^{-\frac{1}{2}}\left\|\left(u_f^h-u_p^h\right)\cdot n_f\right\|_\Gamma\left\|h^h\right\|, \tag{32}$$

where $C_2=\rho g\,\tilde{C}_{\mathrm{inv}}\tilde{C}_v$ and

$$\frac{\delta}{h}\left(\left(u_f^h-u_p^h\right)\cdot n_f,\left(v_f^h-v_p^h\right)\cdot n_f\right)_\Gamma\le h^{-\frac{1}{2}}\left(\delta\left\|\left(u_f^h-u_p^h\right)\cdot n_f\right\|_\Gamma\left\|\left(v_f^h-v_p^h\right)\cdot n_f\right\|_\Gamma\right). \tag{33}$$

Now we can use (31)–(33) in

$$\begin{aligned}\tilde{L}\left(u_f^h,p^h,u_p^h,h^h;v_f^h,q^h,v_p^h,\psi^h\right)&=a_f\left(u_f^h,v_f^h\right)-b_f\left(v_f^h,p^h\right)+b_f\left(u_f^h,q^h\right)\\&\quad+a_p\left(u_p^h,v_p^h\right)-b_p\left(v_p^h,h^h\right)+b_p\left(u_p^h,\psi^h\right)+c_\Gamma\left(v_f^h-v_p^h,h^h\right)\\&\quad+\frac{\delta}{h}\left(\left(u_f^h-u_p^h\right)\cdot n_f\right)\left(\left(v_f^h-v_p^h\right)\cdot n_f\right)_\Gamma\end{aligned} \tag{34}$$

to complete the proof of the continuity of the stabilized finite element scheme. □

(ii) Coercivity of the stabilized finite element scheme.

Theorem 2. *There exists a constant $\beta>0$ such that the inequality*

$$\sup_{\left(u_f^h,p^h,u_p^h,h^h\right)\in\left(X_{fh},Q_{fh};X_{ph},Q_{ph}\right)}\frac{\tilde{L}\left(u_f^h,p^h,u_p^h,h^h;v_f^h,q^h,v_p^h,\psi^h\right)}{\left|\left\|v_f^h,q^h,v_p^h,\psi^h\right\|\right|}\geq\beta\left|\left\|u_f^h,p^h,u_p^h,h^h\right\|\right| \tag{35}$$

holds for all $\left(v_f^h,q^h,v_p^h,\psi^h\right)\in(X_{fh},Q_{fh},X_{ph},Q_{ph})$.

Proof. In this proof we construct $\left(\hat{v}_f^h,\hat{q}^h,\hat{v}_p^h,\hat{\psi}^h\right)$ such that

$$\tilde{L}\left(u_f^h,p^h,u_p^h,h^h;\hat{v}_f^h,\hat{q}^h,\hat{v}_p^h,\hat{\psi}^h\right)\geq C\left(\left|\left\|u_f^h,p^h,u_p^h,h^h\right\|\right|\right)\left(\left|\left\|\hat{v}_f^h,\hat{q}^h,\hat{v}_p^h,\hat{\psi}^h\right\|\right|\right). \tag{36}$$

For the sake of clarity we divide the proof into steps.

Step 1. Setting $\left(v_f^h,q^h,v_p^h,h^h\right)=\left(u_f^h,p^h,u_p^h,h^h+\nabla\cdot u_p^h\right)$, we obtain

$$\begin{aligned}\tilde{L}\left(u_f^h,p^h,u_p^h,h^h;u_f^h,p^h,u_p^h,\psi^h+\nabla\cdot u_p^h\right)&=\left\|u_f^h\right\|_1^2+\left\|u_f^h\right\|_{\Gamma_f}^2+\left\|u_p^h\right\|_{\mathrm{div}}^2\\&\quad+\frac{\delta}{h}\left\|u_f^h-u_p^h\right\|_\Gamma^2+c_\Gamma\left(u_f^h-u_p^h,h^h\right).\end{aligned} \tag{37}$$

We have

$$\begin{aligned}a_f(u_f^h,u_f^h)&\geq\bar{C}\|u_f^h\|\|u_f^h\|,\\\tilde{L}(u_f^h,p^h,u_p^h,h^h;u_f^h,p^h,u_p^h,\psi^h+\nabla\cdot u_p^h)&\geq\bar{C}\|u_f^h\|_1^2+\|u_p^h\|_{\mathrm{div}}^2\\&\quad+\frac{\delta}{h}\|u_f^h-u_p^h\|_\Gamma^2+c_\Gamma(u_f^h-u_p^h,h^h).\end{aligned} \tag{38}$$

It is easy to see that

$$c_\Gamma\left(u_f^h-u_p^h,h^h\right)\geq-\frac{\left(\rho gC_vC_{\mathrm{inv}}\right)^2}{\gamma hC_2}\left\|\left(u_f^h-u_p^h\right)\cdot n_f\right\|_\Gamma^2-\frac{\gamma C_2}{4}\left\|h^h\right\|^2,$$

where γ is a real positive parameter defined below.

Step 2. Let $\left(v_f^h,q^h,v_p^h,h^h\right)=\left(-\gamma W_f^h,0,-\gamma W_p^h,0\right)$, where W_f^h and W_p^h satisfy (23) and (24), respectively. One can see that, based on the definition $\left\|\left(W_f^h-W_p^h\right)\cdot n_f\right\|_\Gamma=\lambda_3\left\|\left(u_f^h-u_p^h\right)\cdot n_f\right\|_\Gamma$, $\left\|W_f^h\right\|_\Gamma=\lambda_3\left\|u_f^h\right\|_\Gamma$ and the fact that (21)–(24) hold true, we have

$$\begin{aligned}\tilde{L}\left(u_f^h,p^h,u_p^h,h^h;-\gamma W_f^h,0,-\gamma W_p^h,0\right)\geq&-\frac{\gamma\lambda_1^2}{2C_1}\left\|u_f^h\right\|_1^2-\frac{\gamma\lambda_2^2}{2}\left\|u_p^h\right\|_{\mathrm{div}}^2\left\|h^h\right\|+\frac{\gamma C_1}{2}\left\|p^h\right\|^2\\&+\gamma C_2\left\|h^h\right\|^2-\frac{\gamma\delta\lambda_3}{h}\left\|\left(u_f^h-u_p^h\right)\cdot n_f\right\|_\Gamma^2\\&-\frac{\gamma\lambda_3^2\rho^2g^2\hat{C}_v^2\hat{C}_{\mathrm{inv}}^2}{hC_2}\left\|\left(u_f^h-u_p^h\right)\cdot n_f\right\|_\Gamma^2,\end{aligned}$$

where δ is a real parameter defined in the next step.

Let us use the following two Young properties:

$$\gamma\lambda_2\|u_p^h\|_{\mathrm{div}}\|h^h\| \le \frac{\gamma\lambda_2^2}{C_2}\|u_p^h\|_{\mathrm{div}}^2 + \frac{\gamma C_2}{4}\|h^h\| \tag{39}$$

and

$$\gamma\lambda_3\rho g\hat{C}_v\hat{C}_{\mathrm{inv}}h^{-\frac{1}{2}}\|(u_f^h - u_p^h)\cdot n_f\|_\Gamma\|h^h\| \le \frac{\gamma\lambda_3^2\rho^2g^2\hat{C}_v^2\hat{C}_{\mathrm{inv}}^2}{hC_2}\|(u_f^h - u_p^h)\cdot n_f\|_\Gamma^2 + \frac{\gamma C_2}{4}\|h^h\|^2.$$

For $a_\Gamma(u_f^h, v_f^h)$ we have the following estimate:

$$0 \le a_\Gamma\left(u_f^h, v_f^h\right) = \|u_f^h\|_\Gamma \le C_1h^{-\frac{1}{2}}\|u_f^h\|\|v_f^h\|, \tag{40}$$

where $C_1 = C_{\mathrm{inv}}^{\frac{1}{2}}C_v$.

Step 3. Denote $(\hat{v}_f^h, \hat{q}^h, \hat{v}_p^h, \hat{h}^h) = (u_f^h - \gamma w_f^h, p^h, u_p^h - \gamma w_p^h, \psi^h + \nabla\cdot u_p^h)$ and $\tilde{L}^h = \tilde{L}(u_f^h, p^h, u_p^h, h^h; u_f^h - \gamma w_f^h, p^h, u_p^h - \gamma w_p^h, \psi^h + \nabla\cdot u_p^h)$. Then

$$\begin{aligned}\tilde{L}^h \ge{}& \left(1 - \frac{\lambda_1^2}{2C_1} - \frac{\gamma C_v^2C_{\mathrm{inv}}^2}{hC_2}\right)\|u_f^h\|_1^2 + \left(1 - \frac{\gamma\lambda_2^2}{2C_1}\right)\|u_p^h\|_{\mathrm{div}}^2 + \frac{\gamma C_1}{2}\|p^h\|^2 + \frac{\gamma C_2}{4}\|h^h\|^2\\ &+ \left(\delta\frac{1-\gamma\lambda_3}{h} - \frac{\rho^2g^2\hat{C}_v^2\hat{C}_{\mathrm{inv}}^2}{\gamma hC_2} - \frac{\gamma\lambda_3^2\rho^2g^2\hat{C}_v^2\hat{C}_{\mathrm{inv}}^2}{hC_2}\right)\|\,|u_f^h, p^h, u_p^h, h^h|\,\|^2.\end{aligned} \tag{41}$$

Now we can ensure that the conditions on γ and δ are true by using

$$1 - \bar{C}_1 - \frac{\gamma\lambda_1^2}{C_1} \ge \frac{1}{2}, \quad 1 - \frac{\gamma\lambda_2^2}{C_2} \ge \frac{1}{2}, \quad 1 - \gamma\lambda_3 \ge \frac{1}{4},$$

$$\delta\frac{1-\gamma\lambda_3}{h} - \frac{\rho^2g^2\hat{C}_v^2\hat{C}_{\mathrm{inv}}^2}{\gamma hC_2} - \frac{\gamma\lambda_3^2\rho^2g^2\hat{C}_v^2\hat{C}_{\mathrm{inv}}^2}{hC_2} \ge \frac{\delta}{2h}.$$

We use the parameters γ and δ (where γ is small and δ is large enough):

$$\begin{cases}\gamma \le \min\left\{\left(\dfrac{C_1}{\lambda_1^2} - \dfrac{2C_vC_{\mathrm{inv}}^2C_1}{\lambda_1^2h^{1/2}}\right), \dfrac{2C_2}{\lambda_2^2}, \dfrac{1}{4\lambda_3}\right\},\\ \delta \ge \dfrac{4\rho^2g^2\hat{C}_v^2\hat{C}_{\mathrm{inv}}^2}{\gamma C_2}\left(1 + \gamma^2\lambda_3^2\right).\end{cases}$$

We obtain

$$\begin{aligned}\tilde{L}^h \ge{}& \left(1 - \frac{\lambda_1^2}{2C_1} - \frac{\gamma C_v^2C_{\mathrm{inv}}^2}{hC_2}\right)\|u_f\|_1^2 + \left(1 - \frac{\gamma\lambda_2^2}{2C_1}\right)\|u_p^h\|_{\mathrm{div}}^2 + \frac{\gamma C_1}{2}\|p^h\|^2 + \frac{\gamma C_2}{4}\|h^h\|^2\\ &+ \left(\frac{\delta}{h} - \frac{\gamma\delta\lambda_3}{h} - \frac{\rho^2g^2\hat{C}_v^2\hat{C}_{\mathrm{inv}}^2}{\gamma hC_2} - \frac{\gamma\lambda_3^2\rho^2g^2\hat{C}_v^2\hat{C}_{\mathrm{inv}}^2}{hC_2}\right)|||u_f^h, p^h, u_p^h, h^h|||^2\\ &\ge C_4|||u_f^h, p^h, u_p^h, h^h|||\;|||u_f^h - \gamma w_f^h, p^h, u_p^h - \gamma w_p^h, \psi^h + \nabla\cdot u_p^h|||\\ &= C|||u_f^h, p^h, u_p^h, h^h|||\;|||\hat{u}_f^h, \hat{p}^h, \hat{u}_p^h, \hat{\psi}^h|||.\end{aligned}$$

This concludes the proof of this theorem. □

6. ERROR ESTIMATE

Now we can derive the error estimate. This estimate is based on the continuity and coercivity of the stabilized finite element scheme.

Theorem 3. *Let (u_f, p, u_p, h) be the exact solution and $\left(u_f^h, p^h, u_p^h, h^h\right)$ be the stabilized finite element solution; $\|u_f\|_2$, $\|p\|$, $\|u_p\|_2$ and $\|h\|$ are bounded norms. We have*

$$\left\|u_f - u_f^h\right\|_1 + \left\|p - p^h\right\| + \left\|u_p - u_p^h\right\|_{\mathrm{div}} + \left\|h - h^h\right\| \leq Ch,$$

for all $(u_f, p, u_p, h) \in (X_f, Q_f, X_p, Q_p)$ and $\left(u_f^h, p^h, u_p^h, h^h\right) \in (X_{fh}, Q_{fh}, X_{ph}, Q_{ph})$.

Proof. By subtracting (27) from (14) and using the first equation in (5) on the interface, we define the error equation as follows:

$$\begin{aligned} &L\left(u_f, p, u_p, h; v_f^h, q^h, v_p^h, \psi^h\right) - \tilde{L}\left(u_f^h, p^h, u_p^h, h^h; v_f^h, q^h, v_p^h, \psi^h\right) \\ &= \tilde{L}\left(u_f, p, u_p, h; v_f^h, q^h, v_p^h, \psi^h\right) - \tilde{L}\left(u_f^h, p^h, u_p^h, h^h; v_f^h, q^h, v_p^h, \psi^h\right) \\ &= \tilde{L}\left(u_f - u_f^h, p - p^h, u_p - u_p^h, h - h^h; v_f^h, q^h, v_p^h, \psi^h\right) = 0. \end{aligned} \tag{42}$$

In the view of the interpolation $\left(\bar{u}_f, \bar{p}, \bar{u}_p, \bar{h}\right)$ of the solution (u_f, p, u_p, h) from (X_f, Q_f, X_p, Q_p) into the finite element spaces $(X_{fh}, Q_{fh}, X_{ph}, Q_{ph})$, we can split the errors into two parts:

$$u_f - u_f^h = (u_f - \bar{u}_f) + \left(\bar{u}_f - u_f^h\right) = \bar{e}_f - e_f^h, \tag{43}$$

$$p - p^h = (p - \bar{p}) - \left(\bar{p} - p^h\right) = \bar{\eta} - \eta^h, \tag{44}$$

$$u_p - u_p^h = (u_p - \bar{u}_p) + \left(\bar{u}_p - u_p^h\right) = \bar{e}_p - e_p^h, \tag{45}$$

and

$$h - h^h = \left(h - \bar{h}\right) + \left(\bar{h} - h^h\right) = \bar{\theta} - \theta^h. \tag{46}$$

The interpolation errors are determined as follows:

$$\left\|\bar{e}_f\right\|_1 + \left\|\bar{\eta}\right\| \leq Ch\left(\left\|u_f\right\|_2 + \left\|p\right\|_1\right), \tag{47}$$

$$\left\|\bar{e}_p\right\|_{\mathrm{div}} + \left\|\bar{\theta}\right\| \leq Ch\left(\left\|u_p\right\|_2 + \left\|h\right\|_1\right). \tag{48}$$

We can see that

$$\tilde{L}\left(e_f^h, \eta^h, e_p^h, \theta^h; v_f^h, q^h, v_p^h, \psi^h\right) = -\tilde{L}\left(\bar{e}_f, \bar{\eta}, \bar{e}_p, \bar{\theta}; v_f^h, q^h, v_p^h, \psi^h\right). \tag{49}$$

From the continuity condition in Theorem 1, the coercivity of $\tilde{L}$ in Theorem 2, and the trace and inverse inequalities, we have

$$
\begin{aligned}
\beta\left\|e_f^h,\eta^h,e_p^h,\theta^h\right\| &\leq \sup_{v_f^h,q^h,v_p^h,\psi^h}\frac{\tilde{L}\left(e_f^h,\eta^h,e_p^h,\theta^h;v_f^h,q^h,v_p^h,\psi^h\right)}{\left|\left|\left|v_f^h,q^h,v_p^h,\psi^h\right|\right|\right|}\\
&= \sup_{v_f^h,q^h,v_p^h,\psi^h}\frac{-\tilde{L}\left(\bar{e}_f,\bar{\eta},\bar{e}_p,\bar{\theta};v_f^h,q^h,v_p^h,\psi^h\right)}{\left|\left|\left|v_f^h,q^h,v_p^h,\psi^h\right|\right|\right|}\\
&\leq C\left|\left|\left|\bar{e}_f,\bar{\eta},\bar{e}_p,\bar{\theta}\right|\right|\right|\\
&\leq C\left(\left\|\bar{e}_f\right\|_1+\left\|\bar{\eta}\right\|+\left\|\bar{e}_p\right\|_{\mathrm{div}}+\left\|\bar{\theta}\right\|+h^{-\frac{1}{2}}\left\|\bar{e}_f-\bar{e}_p\right\|_\Gamma\right)\\
&\leq C\left(\left\|\bar{e}_f\right\|_1+\left\|\bar{\eta}\right\|+\left\|\bar{e}_p\right\|_{\mathrm{div}}+\left\|\bar{\theta}\right\|+h^{-1}\left\|\bar{e}_f-\bar{e}_p\right\|_\Gamma\right)\\
&\leq Ch\left(\left\|u_f\right\|_2+\left\|p\right\|_1+\left\|u_p\right\|_2+\left\|h\right\|_1\right).
\end{aligned}
\tag{50}
$$

Finally, from the interpolation error, we deduce estimate (42). □

7. NUMERICAL EXPERIMENTS

In this section, we present results of a numerical experiment based on the mixed finite element method, presented in this article, with application of the simulator Comsol Multiphysics. This simulator using many solvers. In this numerical test we use the MUMPS solver to illustrate the accuracy and efficiency of this method. We consider a global domain $\Omega=[0,1]\times[-0.45,0.15]$ of numerical computations for a coupled system, with a fluid flow region $\Omega_1=[0,1]\times[-0.45,0]$ and porous medium domain $\Omega_2=[0,1]\times[0,0.15]$. The interface in the computational domain is $\Gamma=[0,1]\times\{0\}$.

For the numerical test we take the physical parameters given in Table 1 and the Stokes equation boundary conditions defined as follows:

$$C_{\mu,\beta}:\left(\nabla\mu u_f-pI\right)n_f=0.$$

An injection source $\rho u_p\cdot n_p=1000K$ g/s is placed in the middle left-hand corner of the reservoir and an injection source $\rho u_p\cdot n_p=0$ Kg/s is in the outlet in the top right-hand corner of the domain Ω. The Darcy boundary value problem is defined as follows:

$$u_p\cdot n_p=0.$$

The velocity and the pressure for this problem are calculated using a normal mesh (Fig. 2). We made a comparison with a numerical test with very fine mesh.

Figure 3 illustrates the velocity for our example with a normal mesh and very fine mesh.

Figure 4 shows pressure contours in the fluid flow region with a normal mesh and very fine one. Figure 5 demonstrates pressure contours in porous medium with a normal mesh and very fine one.

To investigate the effect of mesh on the error and convergence of finite element scheme, we perform several numerical tests with different mesh size (Fig. 6).

Table 1. Physical parameters of governing equations

Parameter	Value	Unit
Mass density	1000	kg/m^3
Dynamic viscosity	1	$Pa\cdot s$
Permeability	0.5	m^2
Porosity	0.1	1

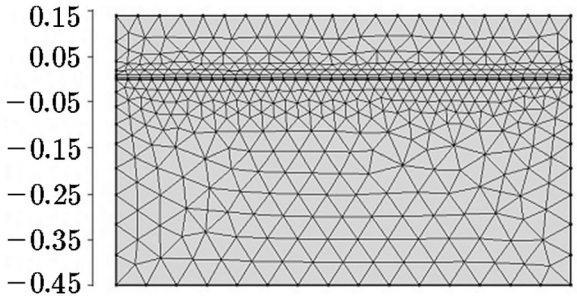

Fig. 2. Normal mesh of domain Ω.

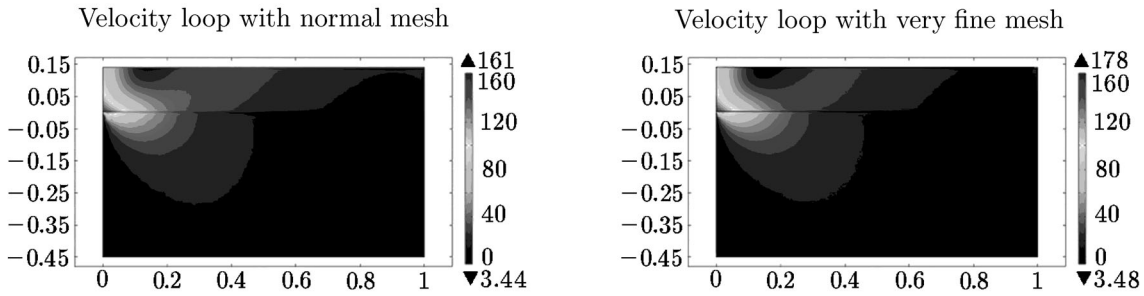

Fig. 3. Velocity contour with using mixed finite element method.

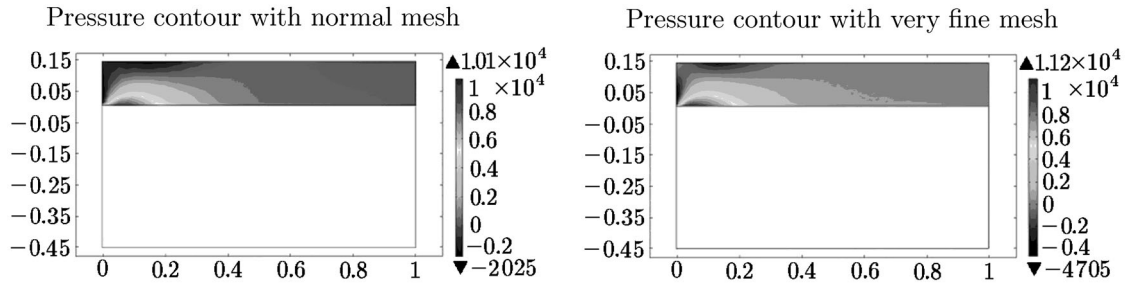

Fig. 4. Pressure contour in Ω_1 with using mixed finite element method.

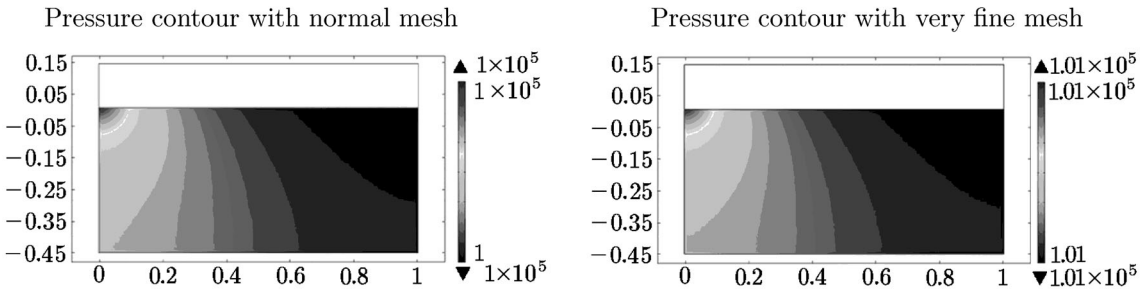

Fig. 5. Pressure contour in Ω_2 with using mixed finite element method.

Table 2 presents different characteristics of the meshes: number of elements and max size and min size of elements.

Now, we will present the variation of the error as a function of the number of iterations for a normal mesh (Fig. 7). To investigate the effect of mesh on the error and convergence for the finite element scheme, we perform several numerical tests at different mesh sizes (see the figures). In these simulations, we use the MUMPS solver, which is very useful for solving large sparse linear systems.

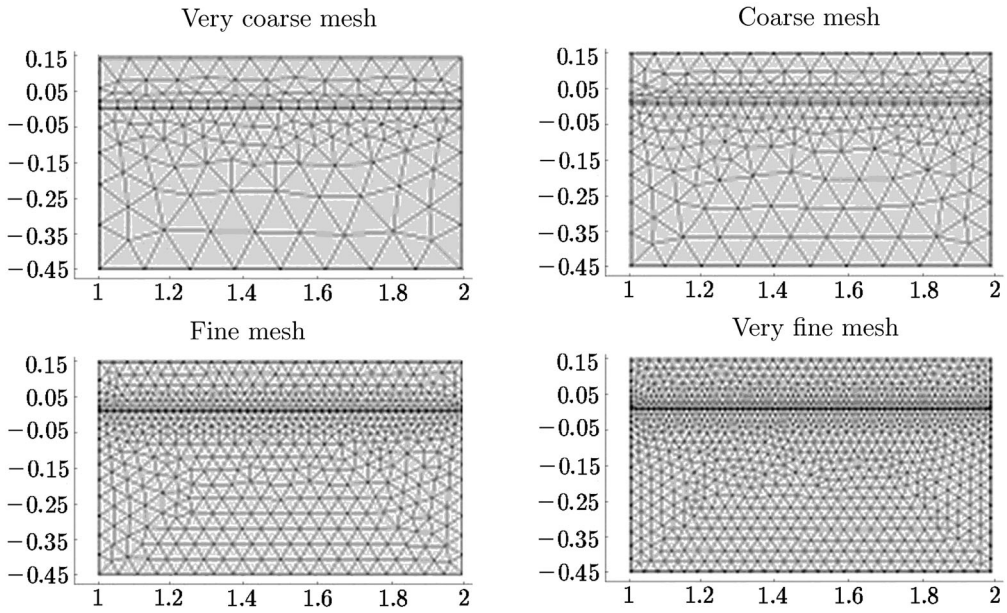

Fig. 6. Different meshes of domain Ω.

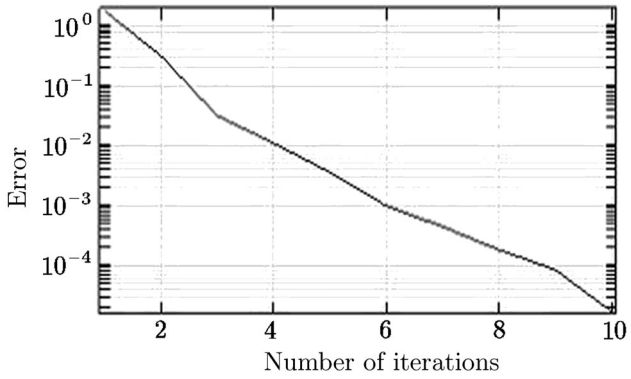

Fig. 7. Error vs. number of iterations for normal mesh.

Table 2. Characteristics of meshes

Mesh	Number of elements	Maximum element size	Minimum element size
Very coarse	306	0.67	0.002
Coarse	487	0.1	$3.0E-4$
Normal	892	0.053	$1.60E-4$
Fine	1331	0.037	$1.25E-4$
Very fine	2267	0.0266	$1.01E-4$

Figure 8 presents the variation of the error as a function of the number of iterations for the mesh presented in Fig. 3.

Figures 7 and 8 show that if the mesh is small, the number of iterations to obtain a good solution is less.

Table 3 presents the errors for our problem on different meshes. Let the error $Erru = \left\|u - u^h\right\|_0$,

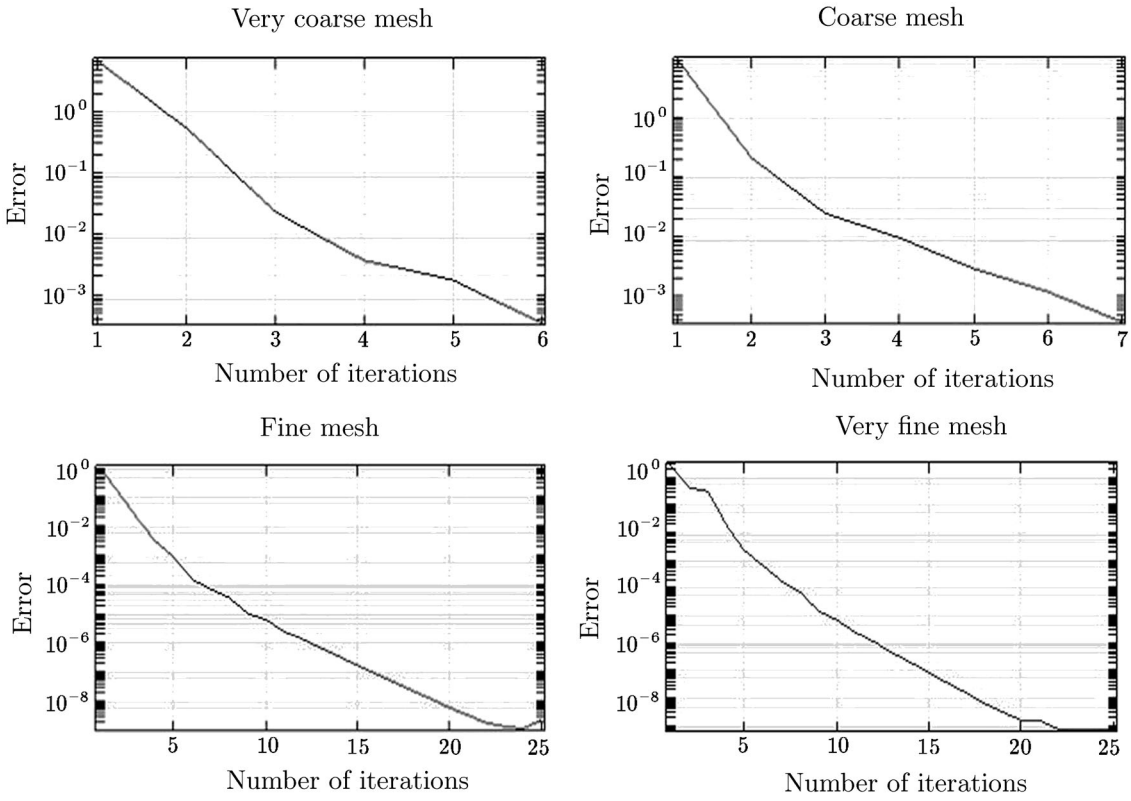

Fig. 8. Error vs. number of iterations for different meshes (Fig. 3.)

Table 3. Errors for the velocity and pressure equations

Numbers of elements	$Erru$	$Errp$
306	0.0013	0.00047
487	0.0011	0.00038
892	0.0008	0.00029
1331	0.00053	0.0002
2267	0.00053	0.00018

where u is the velocity in the fluid flow region, and $Errp = \left\|p - p^h\right\|_0$, where v is the pressure in the porous medium.

Table 3 shows the efficiency of this method; when the mesh is fine enough, the error approaches zero.

8. CONCLUSIONS

In this paper, we investigated application of the mixed finite element method to solve the Stokes–Darcy model with a new boundary condition. In this study, we used discretization of mixed finite element methods to analyze the stability and convergence. We proposed a stabilized finite element scheme. To ensure robustness, we introduce a stabilization term of the temporal discretization. To show the feature of this scheme and the numerical methods, we performed a numerical test on another mesh and compared the results. The numerical test has shown the accuracy and efficiency of the proposed mixed finite element method.

REFERENCES

1. Adams, R.A. and Fournier, J.J.F., *Sobolev Spaces*, 2nd ed., Amsterdam: Elsevier, 2003.
2. Ainsworth, M. and Oden, J., A Posteriori Error Estimators for the Stokes and Oseen Equations, *SIAM J. Num. An.*, 1997, vol. 34, pp. 228–245.
3. Arbogast, T. and Brunson, D.S., A Computational Method for Approximating a Darcy–Stokes System Governing a Vuggy Porous Medium, *Comput. Geosci.*, 2007, vol. 11, pp. 207–218.
4. Arnold, D.N., Brezzi, F., and Fortin, M., A Stable Finite Element for the Stokes Equations, *Calcolo*, 1984, vol. 21, pp. 337–344.
5. Amaziane, B., El Ossmani, M., and Serres, C., Numerical Modeling of the Flow and Transport of Radionuclides in Heterogeneous Porous Media, *Comput. Geosci.*, 2008, vol. 12, pp. 437–449.
6. Babuska, I., Error-Bounds for Finite Element Method, *Numer. Math.*, 1971, vol. 16, pp. 322–333.
7. Badea, L., Discacciati, M., and Quarteroni, A., Numerical Analysis of the Navier–Stokes/Darcy Coupling, *Numerische Math.*, 2010, vol. 115, pp. 195–227.
8. Bank, R.E. and Welfert, B., A Posteriori Error Estimates for the Stokes Problem, *SIAM J. Num. An.*, 1991, vol. 28, pp. 591–623.
9. Benzi, M., Golub, G.H., and Liesen, J., Numerical Solution of Saddle Point Problems, *Acta Numerica*, 2005, vol. 14, pp. 1–137.
10. Boubendir, Y. and Tlupova, S., Domain Decomposition Methods for Solving Stokes–Darcy Problems with Boundary Integrals, *SIAM J. Sci. Comput.*, 2013, vol. 35, pp. B82–B106.
11. Brezzi, F. and Fortin, M., *Mixed and Hybrid Finite Element Methods*, New York: Springer, 1991.
12. Brezzi, F., Douglas, J., Jr., Fortin, M., and Marini, L.D., Efficient Rectangular Mixed Finite Elements in Two and Three Space Variables, *Math. Model. Num. An.*, 1987, vol. 21, pp. 581–604.
13. Brezzi, F., On the Existence, Uniqueness and Approximation of Saddle-Point Problems Arising from Lagrangian Multipliers, *RAIRO: Num. An.*, 1974, vol. 8, pp. 129–151.
14. Burman, E. and Hansbo, P., A Unified Stabilized Method for Stokes' and Darcy's Equations, *J. Comput. Appl. Math.*, 2007, vol. 198, pp. 35–51.
15. Cai, M., Mu, M., and Xu, J., Numerical Solution to a Mixed Navier–Stokes/Darcy Model by the Two-Grid Approach, *SIAM J. Num. An.*, 2009, vol. 47, pp. 3325–3338.
16. Camaño, J., Gatica, G.N., Oyarzúa, R., Ruiz-Baier, R., and Venegas, P., New Fully-Mixed Finite Element Methods for the Stokes–Darcy Coupling, *Comput. Meth. Appl. Mech. Engin.*, 2015, vol. 295, pp. 362–395.
17. Cao, Y., Gunzburger, M., He, X.M., and Wang, X., Robin-Robin Domain Decomposition Methods for the Steady-State Stokes–Darcy System with the Beavers–Joseph Interface Condition, *Numerische Math.*, 2011, vol. 117, pp. 601–629.
18. Cao, Y., Gunzburger, M., Hua, F., and Wang, X., Coupled Stokes–Darcy Model with Beavers–Joseph Interface Boundary Condition, *Commun. Math. Sci.*, 2010, vol. 8, pp. 1–25.
19. Carstensen, C. and Funken, S.A., A Posteriori Error Control in Low-Order Finite Element Discretizations of Incompressible Stationary Flow Problems, *Math. Comput.*, 2001, vol. 70, pp. 1353–1381.
20. Chavent, G. and Jaffre, J., *Mathematical Models and Finite Elements in Reservoir Simulation*, Netherlands: Elsevier, 1986.
21. Discacciati, M., Miglio, E., and Quarteroni, A., Mathematical and Numerical Models for Coupling Surface and Groundwater Flows, *Appl. Num. Math.*, 2002, vol. 43, pp. 57–74.
22. Discacciati, M. and Quarteroni, A., Convergence Analysis of a Subdomain Iterative Method for the Finite Element Approximation of the Coupling of Stokes and Darcy Equations, *Comput. Visualiz. Sci.*, 2004, vol. 6, pp. 93–103.
23. Du, G. and Zuo, L., Local and Parallel Finite Element Method for the Mixed Navier–Stokes/Darcy Model with Beavers–Joseph Interface Conditions, *Acta Mathematica Scientia*, 2017, vol. 37B, pp. 1331–1347.
24. Elakkad, A., Elkhalfi, A., and Guessous, N., An a Posteriori Error Estimate for Mixed Finite Element Approximations of the Navier–Stokes Equations, *J. Korean Math. Soc.*, 2011, vol. 48, no. 3, pp. 529–550.
25. Elman, H., Silvester, D., and Wathen, A., *Finite Elements and Fast Iterative Solvers with Applications in Incompressible Fluid Dynamics*, 2nd ed., Oxford: Oxford Univ. Press, 2014.
26. Gatica, G.N., Oyarzúa, R., and Sayas, F.J., Analysis of Fully-Mixed Finite Element Methods for the Stokes–Darcy Coupled Problem, *Math. Comput.*, 2011, vol. 80, pp. 1911–1948.
27. Gatica, G.N., Oyarzúa, R., and Sayas, F.J., Convergence of a Family of Galerkin Discretizations for the Stokes–Darcy Coupled Problem, *Num. Meth. Part. Diff. Eqs.*, 2011, vol. 27, pp. 721–748.
28. Ghia, U., Ghia, K., and Shin, C., High-Re Solutions for Incompressible Flow Using the Navier–Stokes Equations and a Multigrid Method, *J. Comput. Phys.*, 1982, vol. 48, pp. 387–395.
29. Girault, V. and Rivière, B., DG Approximation of Coupled Navier–Stokes and Darcy Equations by Beaver–Joseph–Saffman Interface Condition, *SIAM J. Num. An.*, 2009, vol. 47, pp. 2052–2089.

30. He, X.M., Li, J., Lin, Y.P., and Ming, J., A Domain Decomposition Method for the Steady-State Navier–Stokes–Darcy Model with the Beavers–Joseph Interface Condition, *SIAM J. Sci. Comput.*, 2015, vol. 37, pp. S264–S290.
31. Hecht, F., Pironneau, O., Le Hyaric, A., and Ohtsuka, K., Freefem++, URL: http://www.freefem.org/ff++.
32. *Incompressible Computational Fluid Dynamics*, Gunzburger, M. and Nicolaides, R., Eds., Cambridge: Cambridge Univ. Press, 1993.
33. Lipnikov, K., Vassilev, D., and Yotov, I., Discontinuous Galerkin and Mimetic Finite Difference Methods for Coupled Stokes–Darcy Flows on Polygonal and Polyhedral Grids, *Numerische Math.*, 2014, vol. 126, pp. 321–360.
34. Mu, M. and Xu, J., A Two-Grid Method of a Mixed Stokes–Darcy Model for Coupling Fluid Flow with Porous Media Flow, *SIAM J. Num. An.*, 2007, vol. 45, pp. 1801–1813.
35. Mu, M. and Zhu, X., Decoupled Schemes for a Non-Stationary Mixed Stokes–Darcy Model, *Math. Comput.*, 2010, vol. 79, pp. 707–731.
36. Payne, L.E. and Straughan, B., Analysis of the Boundary Condition at the Interface between a Viscous Fluid and a Porous Medium and Related Modelling Questions, *J. Math. Pures Appl.*, 1998, vol. 77, pp. 317–354.
37. Pearson, J.W., Pestana, J., and Silvester, D.J., Refined Saddle-Point Preconditioners for Discretized Stokes Problems, *Numerische Math.*, 2018, vol. 138, pp. 331–363; DOI: 10.1007/s00211-017-0908-4.
38. Roberts, J. and Thomas, J.M., in *Mixed and Hybrid Methods, Handbook of Numerical Analysis*, Ciarlet, P. and Lions, J., Eds., vol. II: *Finite Element Methods* (part I), North Holland, 1990, pp. 523–639.
39. Rui, H. and Zhang, R., A Unified Stabilized Mixed Finite Element Method for Coupling Stokes and Darcy Flows, *Comput. Meth. Appl. Mech. Engin.*, 2009, vol. 198, pp. 2692–2699.
40. Saffman, P., On the Boundary Condition at the Surface of a Porous Medium, *Stud. Appl. Math.*, 1971, vol. 50, pp. 93–101.
41. Shan, L. and Zheng, H., Partitioned Time Stepping Method for Fully Evolutionary Stokes–Darcy Flow with Beavers–Joseph Interface Conditions, *SIAM J. Num. An.*, 2013, vol. 51, pp. 813–839.
42. Urquiza, J.M., N'Dri, D., Garon, A., and Delfour, M.C., Coupling Stokes and Darcy Equations, *Appl. Num. Math.*, 2008, vol. 58, pp. 525–538.
43. Zuo, L. and Hou, Y., A Decoupling Two-Grid Algorithm for the Mixed Stokes–Darcy Model with the Beavers–Joseph Interface Condition, *Num. Meth. Part. Diff. Eqs.*, 2014, vol. 30, pp. 1066–1082.
44. Zuo, L. and Hou, Y., A Two-Grid Decoupling Method for the Mixed Stokes–Darcy Model, *J. Comput. Appl. Math.*, 2015, vol. 275, pp. 139–147.
45. Zuo, L. and Hou, Y., Numerical Analysis for the Mixed Navier–Stokes and Darcy Problem with the Beavers–Joseph Interface Condition, *Num. Meth. Part. Diff. Eqs.*, 2015, vol. 31, pp. 1009–1030.